Dual Boundary Element Analysis of Normal Incident Wave Passing a Thin Submerged Breakwater with Rigid, Absorbing, and Permeable Boundaries

Kue-Hong Chen[1]; Jeng-Tzong Chen[2]; Sheng-Yih Lin[3]; and Ying-Te Lee[4]

Abstract: In this paper, the dual integral formulation is derived for solving the scattering problem of normal incident wave passing a thin vertical and inclined barrier with rigid boundary condition which is descending from the water surface to a depth. Absorbing and porous boundary conditions are both considered. The breakwater thickness is assumed to be zero since it is negligible in comparison with the water depth and the wavelength of the incident wave. Although the multidomain boundary element method (BEM) can solve boundary value problems with degenerate boundaries by dividing the interesting domain into two subdomains, the hypersingular formulation provides the key to solve the problem more efficiently in a single domain. To demonstrate the effects of the breakwater with rigid, absorbing, and porous boundary conditions for the energy dissipation by the barrier, the transmission and reflection coefficients of the scattering problem are determined by the developed dual BEM program. In addition, the results are obtained for the cases of wave scattering by the barrier with zero thickness in constant water depth and are compared with the analytical solutions, the multidomain BEM solution, and the experimental data.

DOI: 10.1061/(ASCE)0733-950X(2004)130:4(179)

CE Database subject headings: Boundaries; Boundary element method; Breakwaters; Water depth.

Introduction

The boundary integral equation method (BIEM) or boundary element method (BEM) is now establishing a position as an actual alternative to the finite element method in many fields of engineering. Over the past 20 years, main applications of BIEM or BEM were limited in boundary value problems without degenerate boundaries. Since the degenerate boundary results in rank deficiency for the influence matrix by using the conventional BEM, the multidomain BEM was utilized to solve the nonunique solution by introducing an artificial boundary in the last decade, e.g., cutoff wall (Lafe et al. 1980), thin barrier. (Liu and Abbaspour 1982), screen acoustics (Chen et al. 2003), and crack problems (Blandford et al. 1981). Instead of using the multidomain BEM, the hypersingular formulation plays a key role in solving the problem in a single domain (Chen and Chen 1998). The dual BEM (DBEM) or so-called the dual BIEM developed by Hong and Chen (1988), is becoming very popular for the problems with a degenerate boundary. Aliabadi and his co-worker have extended the DBEM applications and published many papers (Aliabadi 1997, Aliabadi and Saleh 2002). The drawback of the multidomain approach is obvious in that the artificial boundary is arbitrary, and thus not qualified as an automatic scheme. For the computational efficiency, a larger system of equations is required since the degrees of freedoms on the interface are put into the system, and it takes more CPU time and memory space than the DBEM method to solve the linear algebraic equation. Furthermore, the artificial boundary cannot be obtained for a half plane or infinite problem with degenerate boundary. The disadvantages of multidomain encourage researchers to deal with the degenerate boundary problem by using the DBEM in a single domain with hypersingularity in the last decades.

The type of breakwater can be considered as a thin barrier with a rigid boundary condition descending from the water surface to a depth as shown in Fig. 1(a). The effectiveness of zero-thickness breakwater has been examined by various researchers numerically by using the multidomain BEM (Wiegel 1960; Raichlen and Lee 1978; Jones et al. 1979; Liu and Abbaspour 1982). The analytical solution of a vertical thin barrier for the transmission coefficient T was solved in deep water by Ursell (1974). It is interesting that the transmission coefficient becomes very small when $2\pi d/\lambda$ is great than one, where λ is the wavelength and d is the height of the barrier which is descending from the water surface to a depth. For the intermediate and shallow water depth cases, Wiegel (1960) obtained an approximate solution by using the small amplitude wave theory. After comparing with the two solutions, Wiegel's solution does not match well with Ursell's solution in the deep water situation. Other analytical solutions have also been developed by Losada et al. (1992) on the basis of the eigenfunc-

[1]Assistant Professor, Dept. of Information Management, Toko Univ., Chai-Yi, 603, Taiwan, Republic of China. E-mail: khc6177@yahoo.com.tw

[2]Professor, Dept. of Harbor and River Engineering, National Taiwan Ocean Univ., Keelung 20224, Taiwan, Republic of China (corresponding author). E-mail: jtchen@mail.ntou.edu.tw

[3]Graduate Student, Dept. of Harbor and River Engineering, National Taiwan Ocean Univ., Keelung 20224, Taiwan, Republic of China. E-mail: m91520022@mail.ntou.edu.tw

[4]Graduate Student, Dept. of Harbor and River Engineering, National Taiwan Ocean Univ., Keelung 20224, Taiwan, Republic of China. E-mail: m91520022@mail.ntou.edu.tw

Note. Discussion open until December 1, 2004. Separate discussions must be submitted for individual papers. To extend the closing date by one month, a written request must be filed with the ASCE Managing Editor. The manuscript for this paper was submitted for review and possible publication on December 11, 2002; approved on November 21, 2003. This paper is part of the ***Journal of Waterway, Port, Coastal, and Ocean Engineering***, Vol. 130, No. 4, July 1, 2004. ©ASCE, ISSN 0733-950X/2004/4-179–190/$18.00.

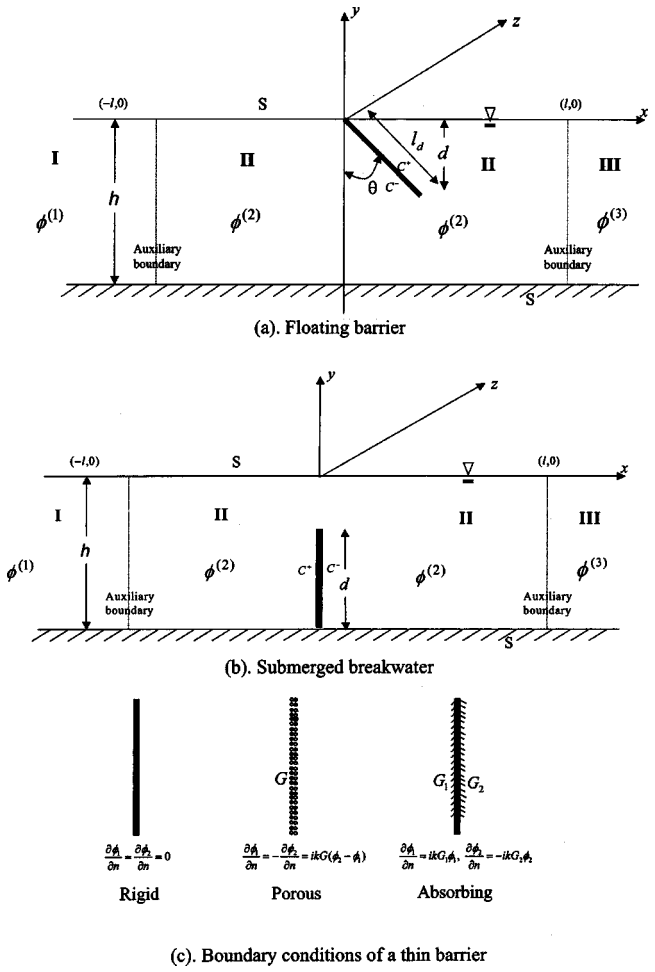

Fig. 1. Definition sketch for two types of thin barrier and their boundary conditions: (a) Floating barrier; (b) submerged breakwater; and (c) boundary conditions of thin barrier

tion expansion method for the case with a vertical thin barrier.

The diffraction of water waves by a thin porous breakwater (degenerate boundary) is considered initially by Yu (1995) and has been widely studied by Losada et al. (1997), Yip and Chwang (1998), McIver (1999), Wu et al. (1999), Lee and Chwang (2000), and Linton and McIver (2000) by using analytical methods. This boundary condition on the breakwater assumes that the normal derivative of the potential of the flow through the breakwater is proportional to the difference in potential across the breakwater. The scattering problem with the finite thickness of the permeable breakwater has been treated by adopting the conventional BEM (Hsu and Wu 1999). The absorbing boundary with different absorbing parameters on the front and back sides of the breakwater has been studied by using the eigenfunction expansion method (Tsaur et al. 2000). To the best of the authors' knowledge, DBEM was never utilized to treat scattering problems of a thin (zero-thickness) breakwater with porous or absorbing boundary condition.

In this paper, we will construct the dual integral formulation in a single domain instead of using the multidomain BEM for solving the problem of normal incident wave passing a thin vertical and inclined barrier with a rigid boundary condition which is descending from the water surface to a depth in Fig. 1(a), and a thin vertical submerged breakwater with absorbing and porous boundary condition which is extending from the seabed to a height in Fig. 1(b), and the rigid, permeable, and absorbing boundary conditions of a thin barrier in Fig. 1(c). After discretizing the dual integral equations, a dual BEM program will be developed to solve wave scattering problems for a zero-thickness breakwater. The results will be compared with those of numerical solutions by using the multidomain BEM (Liu and Abbaspour 1982), the experimental data and the analytical solutions (Ursell 1974; Losada et al. 1992; Tsaur et al. 2000).

Mathematical Formulation

The boundary value problem for the scattering of small amplitude waves by a fixed thin barrier is summarized below (Liu and Abbaspour 1982; Chen et al. 2002). A thin barrier parallel to the z axis is shown in Figs. 1(a and b). A wave train with a frequency σ propagates towards the barrier in a constant water depth h. Assuming inviscid, incompressible fluid and irrotational flow, the wave field may be represented by the velocity potential $\Phi(x,y,t)$ everywhere in the interested domain that satisfies the Laplace equation as

$$\nabla^2\Phi(x,y,t)=0 \tag{1}$$

According to the uniformity of the water depth in the z axis and the periodicity in time, the potential $\Phi(x,y,t)$ of fluid motion can be expressed as

$$\Phi(x,y,t)=\phi(x,y)e^{-i\sigma t} \tag{2}$$

where σ satisfies the dispersion relation

$$\sigma^2=gk\tanh(kh), \tag{3}$$

in which k = wave number; and g = acceleration of gravity. The unknown function $\phi(x,y)$ describes the fluctuation of the potential on the xy plane. Substitution of Eq. (2) into Eq. (1) yields the two-dimensional Laplace equation as follows:

$$\nabla^2\phi(x,y)=0,\ (x,y)\ \text{ in }\ D \tag{4}$$

where D = domain of interest. The boundary conditions of the interested domain are summarized as follows:

1. The linearized free water surface boundary condition (Dean and Dalrymple 1984)

$$\frac{\partial\phi}{\partial y}-\frac{\sigma^2\phi}{g}=0 \tag{5}$$

2. Seabed boundary conditions

$$\frac{\partial\phi}{\partial n}=0 \tag{6}$$

where n = boundary normal vector. The bottom is impermeable.

3. Breakwater boundary conditions.
   - Rigid boundary condition [as shown in Fig. 1(c)]

$$\frac{\partial\phi_1}{\partial n}=\frac{\partial\phi_2}{\partial n}=0 \tag{7}$$

where subscripts 1 and 2 denote the front and back sides of the breakwater, respectively. The normal velocity is zero on the barrier.

   - Porous boundary condition [as shown in Fig. 1(c)]

$$\frac{\partial\phi_1}{\partial n}=-\frac{\partial\phi_2}{\partial n}=ikG(\phi_2-\phi_1) \tag{8}$$

where G = complex porous-wall-effect parameter (Yu 1995),

and indicates that the fluid velocity normal to the barrier is proportional to the pressure difference across the barrier. The real part of G is the resistance of the barrier and the imaginary part is the phase differences between the velocity and the pressure due to inertial effects. The resistance may be related with a friction coefficient or a head loss coefficient. Inertial effects may be related with an added mass coefficient or effective bore diameter.

- Absorbing boundary condition [as shown in Fig. 1(c)]

$$\frac{\partial \phi_1}{\partial n} = ikG_1\phi_1 \tag{9}$$

$$\frac{\partial \phi_2}{\partial n} = -ikG_2\phi_2 \tag{10}$$

where G_1 and G_2 = absorbing parameters of the front and back sides of the breakwater. This barrier can reduce kinetic energy of incident water wave by placing armor unit with different absorbing parameters on the front side and back side of the breakwater

4. Radiation condition at infinity (Sommerfeld 1964)

$$\lim_{r\to\infty} r^{1/2}\left(\frac{\partial \phi}{\partial r} - ik\phi\right) = 0 \tag{11}$$

where $r=\sqrt{x^2+y^2}$. Eq. (11) indicates that the behavior of scattered water wave must be outgoing away from the breakwater structure.

5. The boundary conditions on the fictitious interfaces.

For the infinite strip problem, the domain can be divided into three regions after introducing two pseudoboundaries on both sides of the barrier, $x=\pm l$, as shown in Figs. 1(a and b). The potential in Region I without energy loss can be expressed as

$$\phi^{(1)}(x,y) = -\frac{igA}{\sigma}(e^{ik(x+l)} + \mathrm{Re}^{-ik(x+l)})\frac{\cosh(k(h+y))}{\cosh(kh)} \tag{12}$$

where the superscript (1) denotes the region number; A = amplitude of incident wave; and R = reflection coefficient. The potential in Region III without energy loss which needs to satisfy the radiation B.C. in Eq. (11) can be expressed as

$$\phi^{(3)}(x,y) = -Te^{ik(x-l)}\frac{\cosh(k(h+y))}{\cosh(kh)}\frac{igA}{\sigma} \tag{13}$$

where T = transmission coefficient.

The boundary conditions on the fictitious interfaces are

$$\phi^{(1)}(-l,y) = \phi^{(2)}(-l,y) \tag{14}$$

$$\left.\frac{\partial \phi^{(1)}}{\partial x}\right|_{x=-l} = \left.\frac{\partial \phi^{(2)}}{\partial x}\right|_{x=-l} \tag{15}$$

$$\phi^{(3)}(l,y) = \phi^{(2)}(l,y) \tag{16}$$

$$\left.\frac{\partial \phi^{(3)}}{\partial x}\right|_{x=l} = \left.\frac{\partial \phi^{(2)}}{\partial x}\right|_{x=l} \tag{17}$$

According to Eqs. (12), (13), (14), and (16), we can derive the reflection and transmission coefficients as follows:

$$R = -1 + \frac{k}{n_0\sinh(kh)}\int_{-h}^{0}\phi^{(2)}(-l,y)\cosh(k(h+y))dy \tag{18}$$

$$T = \frac{k}{n_0\sinh(kh)}\int_{-h}^{0}\phi^{(2)}(l,y)\cosh(k(h+y))dy \tag{19}$$

where

$$n_0 = \frac{1}{2}\left(1 + \frac{2kh}{\sinh(2kh)}\right)$$

Dual Boundary Integral Equations for Wave Scattering by Thin Barrier

The first equation of the dual boundary integral equations for the domain point can be derived from the Green's third identity (Chen and Hong 1993)

$$2\pi\phi(\tilde{x}) = \int_B T(\tilde{s},\tilde{x})\phi(\tilde{s})dB(\tilde{s}) - \int_B U(\tilde{s},\tilde{x})\frac{\partial\phi(\tilde{s})}{\partial n_s}dB(\tilde{s}), \quad \tilde{x}\in D \tag{20}$$

where $\tilde{x}$ = field point ($\tilde{x}=(x,y)$); $\tilde{s}$ = source point; and $U(\tilde{s},\tilde{x})$ and $T(\tilde{s},\tilde{x})$ are

$$U(\tilde{s},\tilde{x}) = \ln(|\tilde{s}-\tilde{x}|)$$

$$T(\tilde{s},\tilde{x}) \equiv \frac{\partial U(\tilde{s},\tilde{x})}{\partial n_{\tilde{s}}} \tag{21}$$

in which $n_{\tilde{s}}$ denotes the normal vector at the boundary point $\tilde{s}$, and $U(\tilde{s},\tilde{x})$ is the fundamental solution which satisfies

$$\nabla^2 U(\tilde{x},\tilde{s}) = \delta(\tilde{x}-\tilde{s}), \quad \tilde{x}\in D \tag{22}$$

where $\delta(\tilde{x}-\tilde{s})$ = Dirac-delta function. After taking normal derivative with respect to Eq. (20) for a thin barrier problem, the second equation of the dual boundary integral formulation for the domain point is derived

$$2\pi\frac{\partial\phi(\tilde{x})}{\partial n_{\tilde{x}}} = \int_B M(\tilde{s},\tilde{x})\phi(\tilde{s})dB(\tilde{s}) - \int_B L(\tilde{s},\tilde{x})\frac{\partial\phi(\tilde{s})}{\partial n_{\tilde{s}}}dB(\tilde{s}), \quad \tilde{x}\in D \tag{23}$$

where

$$L(\tilde{s},\tilde{x}) \equiv \frac{\partial U(\tilde{s},\tilde{x})}{\partial n_{\tilde{x}}} \tag{24}$$

$$M(\tilde{s},\tilde{x}) \equiv \frac{\partial^2 U(\tilde{s},\tilde{x})}{\partial n_{\tilde{x}}\partial n_{\tilde{s}}} \tag{25}$$

in which $n_{\tilde{x}}$ represents the normal vector of $\tilde{x}$. By moving the field point $\tilde{x}$ in Eqs. (20) and (23) to the boundary, the dual boundary integral equations for the boundary point can be obtained as follows:

$$\pi\phi(\tilde{x}) = \mathrm{CPV}\int_B T(\tilde{s},\tilde{x})\phi(\tilde{s})dB(\tilde{s}) - \mathrm{RPV}\int_B U(\tilde{s},\tilde{x})\frac{\partial\phi(\tilde{s})}{\partial n_{\tilde{s}}}dB(\tilde{s}), \quad \tilde{x}\in B \tag{26}$$

$$\pi \frac{\partial \phi(\tilde{x})}{\partial n_{\tilde{x}}} = \text{HPV} \int_B M(\tilde{s},\tilde{x}) \phi(\tilde{s}) dB(\tilde{s}) - \text{CPV} \int_B L(\tilde{s},\tilde{x}) \frac{\partial \phi(\tilde{s})}{\partial n_{\tilde{s}}} dB(\tilde{s}) \quad \tilde{x} \in B \quad (27)$$

where RPV, CPV, and HPV = Riemann principal value, Cauchy principal value, and Hadamard (Mangler) principal values, respectively.

It should be noted that Eq. (27) can be derived simply by applying a normal derivative operator with respect to Eq. (26). Differentiation of the Cauchy principal value should be carried out carefully by using Leibnitz's rule (Chen and Hong 1999). The commutative property provides us with two alternatives for calculating the Hadamard principal value in a similar way used for crack problems (Hong and Chen 1988) and acoustics (Chen and Chen 1998). For the problem including an ordinary boundary S and degenerate boundaries C^+ and C^- on the both sides of a thin barrier as shown in Figs. 1(a and b), i.e., $B = S + C^+ + C^-$, Eqs. (26) and (27) can be reformulated as follows:

For $\tilde{x} \in S$, Eqs. (26) and (27) become

$$\pi \phi(\tilde{x}) = \text{CPV} \int_S T(\tilde{s},\tilde{x}) \phi(\tilde{s}) dB(\tilde{s}) - \text{RPV} \int_S U(\tilde{s},\tilde{x}) \frac{\partial \phi(\tilde{s})}{\partial n_{\tilde{s}}} dB(\tilde{s}) + \int_{C^+} T(\tilde{s},\tilde{x}) \Delta\phi(\tilde{x}) dB(\tilde{s}) - \int_{C^+} U(\tilde{s},\tilde{x}) \Sigma \frac{\partial \phi(\tilde{s})}{\partial n_{\tilde{s}}} dB(\tilde{s}) \quad (28)$$

$$\pi \frac{\partial \phi(\tilde{x})}{\partial n_{\tilde{x}}} = \text{HPV} \int_S M(\tilde{s},\tilde{x}) \phi(\tilde{s}) dB(\tilde{s}) - \text{CPV} \int_S L(\tilde{s},\tilde{x}) \frac{\partial \phi(\tilde{s})}{\partial n_{\tilde{s}}} dB(\tilde{s}) + \int_{C^+} M(\tilde{s},\tilde{x}) \Delta\phi(\tilde{s}) dB(\tilde{s}) - \int_{C^+} L(\tilde{s},\tilde{x}) \Sigma \frac{\partial \phi(\tilde{s})}{\partial n_{\tilde{s}}} dB(\tilde{s}) \quad (29)$$

where

$$\Delta\phi(\tilde{s}) \equiv \phi(\tilde{s}^+) - \phi(\tilde{s}^-) \quad (30)$$

$$\Sigma \frac{\partial \phi}{\partial n}(\tilde{s}) \equiv \frac{\partial \phi}{\partial n}(\tilde{s}^+) + \frac{\partial \phi}{\partial n}(\tilde{s}^-) \quad (31)$$

For $\tilde{x} \in C^+$, Eqs. (26) and (27) reduce to

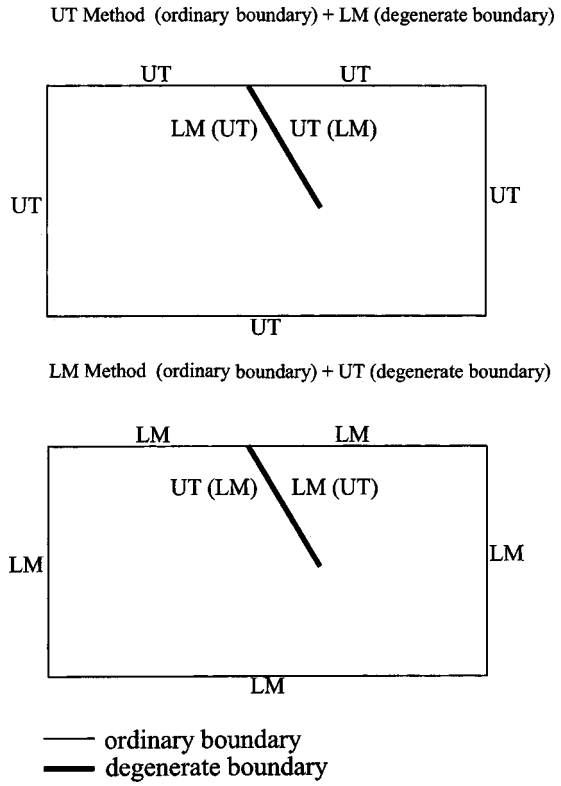

Fig. 2. Two alternative approaches for degenerate-boundary using dual formulation

$$\pi \Sigma \phi(\tilde{x}) = \text{CPV} \int_{C^+} T(\tilde{s},\tilde{x}) \Delta\phi(\tilde{s}) dB(\tilde{s}) - \text{RPV} \int_{C^+} U(\tilde{s},\tilde{x}) \Sigma \frac{\partial \phi(\tilde{s})}{\partial n_{\tilde{s}}} dB(\tilde{s}) + \int_S T(\tilde{s},\tilde{x}) \phi(\tilde{s}) dB(\tilde{s}) - \int_S U(\tilde{s},\tilde{x}) \frac{\partial \phi(\tilde{s})}{\partial n_{\tilde{s}}} dB(\tilde{s}) \quad (32)$$

$$\pi \Delta \frac{\partial \phi(\tilde{x})}{\partial n_{\tilde{x}}} = \text{HPV} \int_{C^+} M(\tilde{s},\tilde{x}) \Delta\phi(\tilde{s}) dB(\tilde{s}) - \text{CPV} \int_{C^+} L(\tilde{s},\tilde{x}) \Sigma \frac{\partial \phi(\tilde{s})}{\partial n_{\tilde{s}}} dB(\tilde{s}) + \int_S M(\tilde{s},\tilde{x}) \phi(\tilde{s}) dB(\tilde{s}) - \int_S L(\tilde{s},\tilde{x}) \frac{\partial \phi(\tilde{s})}{\partial n_{\tilde{s}}} dB(\tilde{s}) \quad (33)$$

where

$$\Sigma\phi(\tilde{s}) \cong \phi(\tilde{s}^+) + \phi(\tilde{s}^-) \quad (34)$$

$$\Delta \frac{\partial \phi}{\partial n}(\tilde{s}) \equiv \frac{\partial \phi}{\partial n}(\tilde{s}^+) - \frac{\partial \phi}{\partial n}(\tilde{s}^-) \quad (35)$$

Eqs. (30), (31), (34), and (35) indicate that the boundary unknowns on the degenerate boundary double, and that the additional hypersingular integral equation, Eq. (23), is correspondingly necessary, i.e., the dual boundary integral equations can

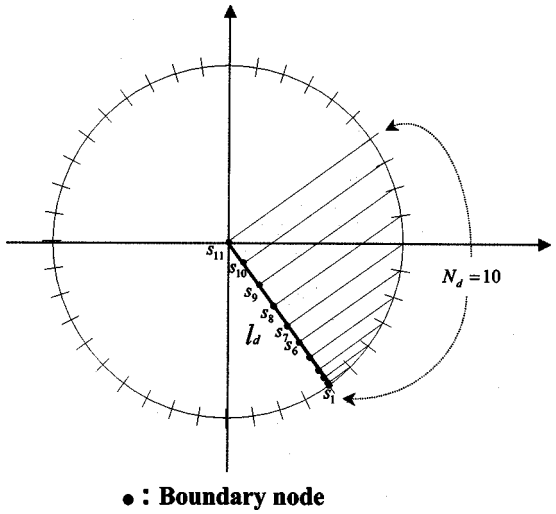

Fig. 3. Chebyshev nodes on thin barrier

provide us with sufficient constraints for the doubled boundary unknowns on the degenerate boundary.

Dual Boundary Element Method for Wave Scattering by Thin Barrier

By discretizing Eqs. (26) and (27) into boundary elements, we can obtain the equations as follows:

$$[\overline{T}_{ij}]\{\phi_j\}=[U_{ij}]\left\{\left(\frac{\partial\phi}{\partial n}\right)_j\right\}$$

$$[M_{ij}]\{\phi_j\}=[\overline{L}_{ij}]\left\{\left(\frac{\partial\phi}{\partial n}\right)_j\right\}$$

where the elements of the four influence matrices are

$$U_{ij}=\mathrm{RPV}\int_{B_j}U(\tilde{s}_j,\tilde{x}_i)dB(\tilde{s}_j) \tag{36}$$

$$\overline{T}_{ij}=-\pi\delta_{ij}+\mathrm{CPV}\int_{B_j}T(\tilde{s}_j,\tilde{x}_i)dB(\tilde{s}_j) \tag{37}$$

$$\overline{L}_{ij}=\pi\delta_{ij}+\mathrm{CPV}\int_{B_j}L(\tilde{s}_j,\tilde{x}_i)dB(\tilde{s}_j) \tag{38}$$

$$M_{ij}=\mathrm{HPV}\int_{B_j}M(\tilde{s}_j,\tilde{x}_i)dB(\tilde{s}_j) \tag{39}$$

in which $\tilde{x}_i=i$th collocation point; $dB(\tilde{s}_j)=j$th integration element; and B_j denotes the jth boundary element. After combining the dual equations on the degenerate boundary when $\tilde{x}$ collocates on C^+ or C^-, the singular system of the four influence matrices are desingularized. Since either one of the two equations, *UT* or *LM*, for the ordinary boundary S can be selected, two alternative approaches, $UT+LM$ and $LM+UT$ in Fig. 2, are proposed.

The $UT+LM$ method employs the following equation:

$$\begin{bmatrix} T_{i_S j_S} & T_{i_S j_{C^+}} & T_{i_S j_{C^-}} \\ T_{i_{C^+} j_S} & T_{i_{C^+} j_{C^+}} & T_{i_{C^+} j_{C^-}} \\ M_{i_{C^+} j_S} & M_{i_{C^+} j_{C^+}} & M_{i_{C^+} j_{C^-}} \end{bmatrix} \begin{Bmatrix} \phi_{j_S} \\ \phi_{j_{C^+}} \\ \phi_{j_{C^-}} \end{Bmatrix}$$

$$= \begin{bmatrix} U_{i_S j_S} & U_{i_S j_{C^+}} & U_{i_S j_{C^-}} \\ U_{i_{C^+} j_S} & U_{i_{C^+} j_{C^+}} & U_{i_{C^+} j_{C^-}} \\ L_{i_{C^+} j_S} & L_{i_{C^+} j_{C^+}} & L_{i_{C^+} j_{C^-}} \end{bmatrix} \begin{Bmatrix} \dfrac{\partial\phi}{\partial n_{j_S}} \\ \dfrac{\partial\phi}{\partial n_{j_{C^+}}} \\ \dfrac{\partial\phi}{\partial n_{j_{C^-}}} \end{Bmatrix} \tag{40}$$

where i_S and i_{C^+} denote the collocation points on the S and C^+ boundaries, respectively, and j_S and j_{C^+} denote the element I.D. on the S and C^+ boundaries, respectively. Besides, the $LM+UT$ method can solve the degenerate boundary problem by using

$$\begin{bmatrix} M_{i_S j_S} & M_{i_S j_{C^+}} & M_{i_S j_{C^-}} \\ T_{i_{C^+} j_S} & T_{i_{C^+} j_{C^+}} & T_{i_{C^+} j_{C^-}} \\ M_{i_{C^+} j_S} & M_{i_{C^+} j_{C^+}} & M_{i_{C^+} j_{C^-}} \end{bmatrix} \begin{Bmatrix} \phi_{j_S} \\ \phi_{j_{C^+}} \\ \phi_{j_{C^-}} \end{Bmatrix}$$

$$= \begin{bmatrix} L_{i_S j_S} & L_{i_S j_{C^+}} & L_{i_S j_{C^-}} \\ U_{i_{C^+} j_S} & U_{i_{C^+} j_{C^+}} & U_{i_{C^+} j_{C^-}} \\ L_{i_{C^+} j_S} & L_{i_{C^+} j_{C^+}} & L_{i_{C^+} j_{C^-}} \end{bmatrix} \begin{Bmatrix} \dfrac{\partial\phi}{\partial n_{j_S}} \\ \dfrac{\partial\phi}{\partial n_{j_{C^+}}} \\ \dfrac{\partial\phi}{\partial n_{j_{C^-}}} \end{Bmatrix} \tag{41}$$

The main difference between Eqs. (40) and (41) is the constraint obtained by collocating the points on the ordinary boundary (S), using the *UT* and *LM* equations, respectively.

In the numerical implementation, the velocity field is singular at the tip of the barrier which needs fine mesh. To put more nodes on the near tip of the barrier ($y=-d$) for Eqs. (20) and (23) of the dual boundary integral equations, the Chebyshev mesh is adopted by

$$s_i=-l_d\cos(i-1)\frac{\pi}{n_d},\quad i=1,\ldots,n_d+1 \tag{42}$$

where $s_i=$coordinate of boundary node on the barrier; and l_d and $n_d=$length and total numbers of elements on the barrier. The Chebyshev mesh accumulates nodes near the end of the barrier as shown in Fig. 3, and allocation of the mesh points is an adaptive scheme on the barrier.

Illustrative Examples

To demonstrate the validity of the dual boundary integral formulation and the developed DBEM program, four examples are given as follows.

Case 1: Floating Vertical Barrier with Rigid Boundary

The boundary element mesh of the scattering water wave problem is shown in Fig. 4. To compare the accuracy of the DBEM results ($UT+LM$ or $LM+UT$) with the analytical solution of the deep

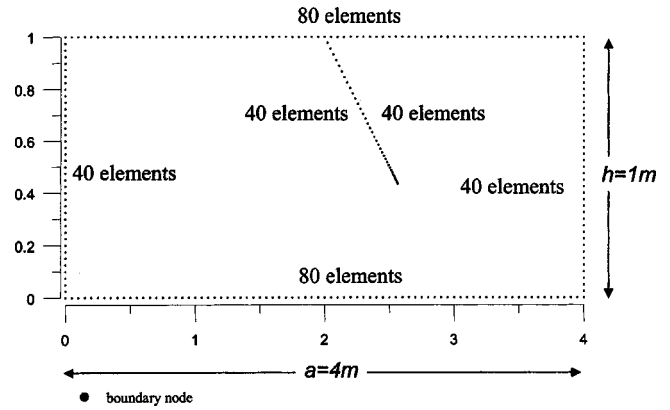

Fig. 4. Boundary element mesh

water theorem by Ursell (1974) and the multidomain BEM results (Liu and Abbaspour 1982) under the deep water condition, the transmission coefficients T and reflection coefficients R against kd are plotted in Fig. 5 for $kh=5$, in which d is the submerged depth of the vertical barrier. The agreement among the present numerical results, the multidomain BEM result and the theoretical solutions is good. The DBEM program is also applied to the cases of intermediate water depth where Wiegel (1960) presented some experimental data. Figs. 6, 7, and 8 show the transmission coefficients T versus d/h for different water depths, $kh=4.272$, 2.1362, and 1.06, respectively. When the solved problem cuts apart into two different domains for $d=L$, the DBEM method is not required when $d=L$. The analytical solution of eigenfunction expansion method by Losada et al. (1992), Wiegel's approximate theoretical solution, and the numerical solution of the multidomain BEM are also shown for comparison. It is found that the solution of DBEM is closer to that of the eigenfunction expansion method than the solution of multidomain BEM. Wiegel's approximate solution (1960) does not work well for the deep water region in Fig. 6. The present numerical results agree well with the results of experimental data and the multidomain BEM well for the cases of intermediate water depth in Figs. 7 and 8. The power transmission theory is the one that captures the trend of the experiments in

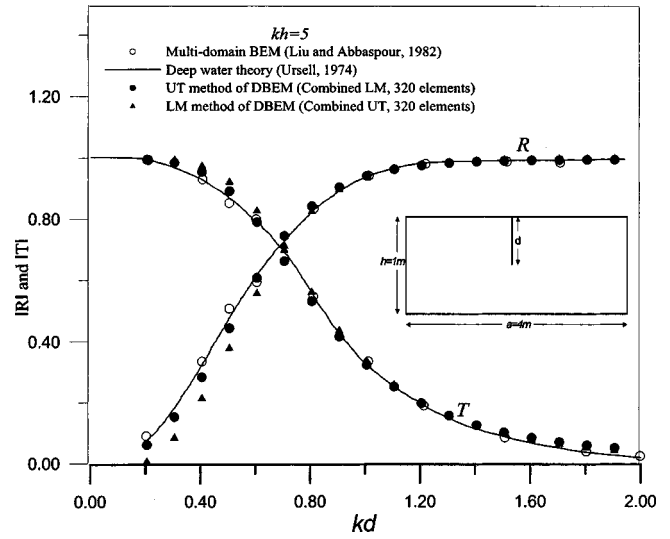

Fig. 5. Transmission and reflection coefficients for different submerged lengths of thin vertical breakwater (case 1, $kh=5$)

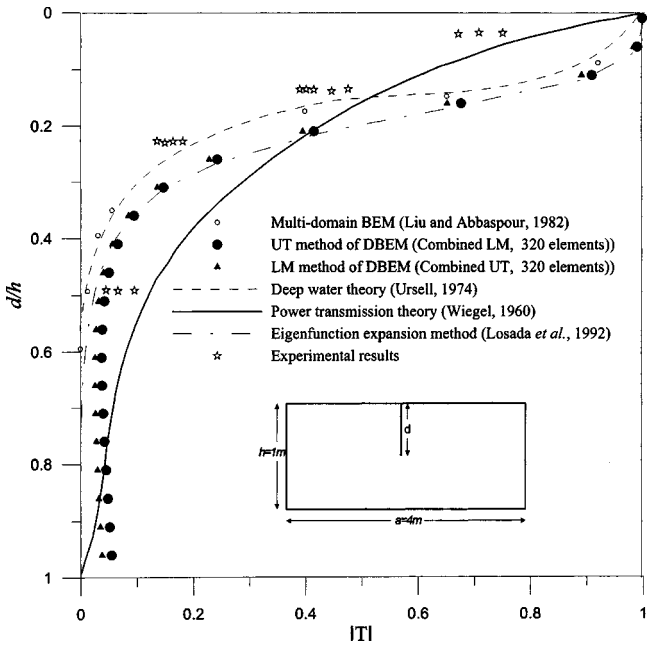

Fig. 6. Transmission coefficients obtained by using different methods (case 1, $kh=4.272$)

the intermediate and shallow water depth cases in Figs. 7 and 8. But the others are closer to the experiments in the deep water situation in Fig. 6. The result is difficult to converge a more reasonable solution when d gets very close to h. We need a more refined mesh to make the grid convergence for the singular behavior of the local area. Therefore, a more reasonable result is obtained by adding more elements in Fig. 8.

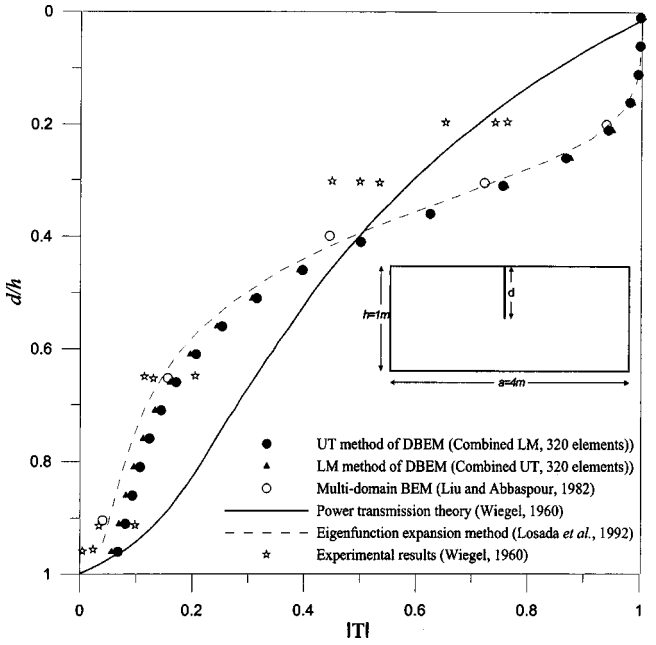

Fig. 7. Transmission coefficients obtained by using different methods (case 1, $kh=2.1362$)

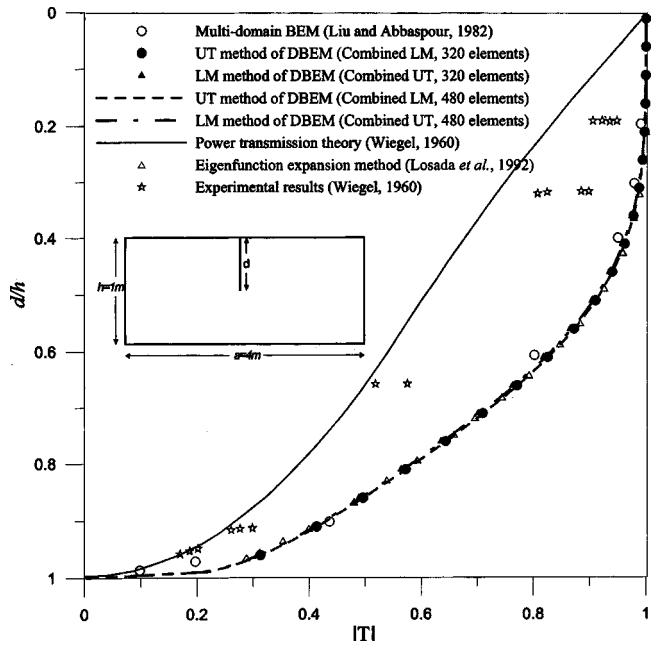

Fig. 8. Transmission coefficients obtained by using different methods (case 1, $kh=1.06$)

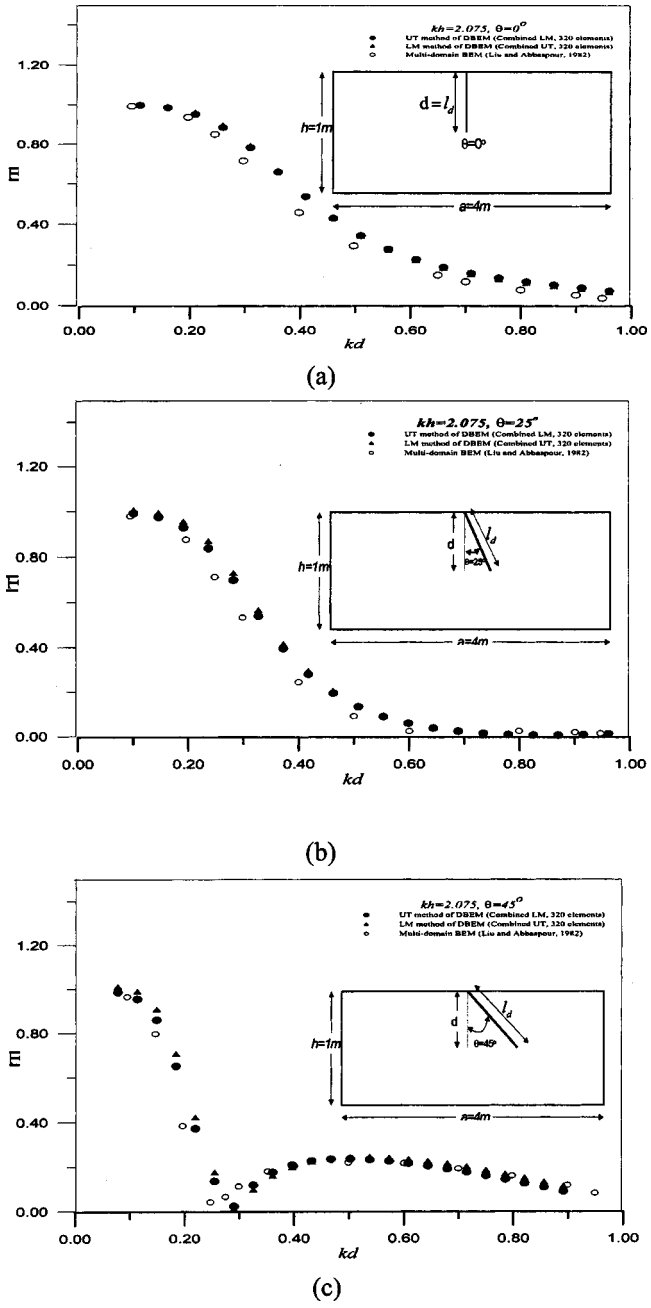

Fig. 9. Transmission coefficients versus submerged depths of thin breakwaters with various angles: (a) $\theta=0°$, (b) $\theta=25°$, (c) $\theta=45°$ (case 2, $kh=2.075$)

Case 2: Floating Inclined Barrier with Rigid Boundary

Numerical experiments were performed to examine the efficiency of an inclined barrier as compared with a vertical barrier. The numerical results of the multidomain BEM are also shown for comparison. The transmission coefficient T versus d/h is plotted for different angles of inclination of $kh=2.075$, $\theta=0°$ in Fig. 9(a), $\theta=25°$ in Fig. 9(b), and $\theta=45°$ in Fig. 9(c). The two solutions, $UT+LM$ and $LM+UT$ approaches, match well with the multidomain BEM solution in Figs. 9(a–c). In fact, the barrier is extremely effective at $d/h=0.285$ for $\theta=45°$ in Fig. 9(c). The transmission coefficient T is plotted against θ for $kh=2.075$, as shown in Figs. 10(a and b), one is for fixed length of the barrier ($l_d/h=0.4$), in which l_d is the length of the barrier; the other is for a fixed gap ($d/h=0.4$). Therefore, the two cases are the same when $\theta=0°$. The present numerical results agree well with those of the multidomain BEM for the cases in Figs. 10(a and b). The numerical results show that the transmission coefficient T is a symmetric function of θ. The barrier acts as a beach when θ is a negative value in the real world. The wave breaking could occur and it could reduce the transmitted wave energy. The free surface profiles on the left side of the barrier are shown in Fig. 11(a) for $\theta=0°$, Fig. 11(b) for $\theta=45°$, and Fig. 11(c) for $\theta=-45°$. The present numerical results agree well with those of the multidomain BEM for the cases in Figs. 11(a–c). For the case of $\theta=0°$ (vertical barrier) in Fig. 11(a), the surface profile is similar to a standing wave. The wave runup phenomenon is clearly revealed for $\theta=-45°$ in Fig. 11(c).

Case 3: Submerged Breakwater with Porous Boundary Condition

Numerical experiments were performed to examine the efficiency of a thin (zero thickness) submerged breakwater with porous boundary condition by varying different porous coefficients. The barrier is modeled as zero thickness, i.e., the barrier is a degenerate boundary. Dual formulation is the key to solving the problem. To verify the accuracy, the results of the eigenfunction expansion method (Tsaur et al. 2000) are also shown for comparison. According to numerical experiments, the length of each pseudoboundary is adopted by the double of water depth. In this case, the submergence ratio (d/h) is 0.75. By using the dual formulations (*UT* or *LM* method), the reflection and transmission coefficients are plotted against *kh* in Figs. 12 and 13 for $G=0.5$ and $G=1.0$ in Eq. (8), respectively. The results compare well with the eigenfunction expansion method. To see the dissipation efficiency due to porous parameters, transmission and reflection coefficients with different porous coefficients, $G=0$, 0.5, and 1.0, versus *kh* by using the *UT* method (combined with the *LM* method) are shown in Fig. 14. The physical phenomenon of energy-loss dependency for different porous materials is clearly

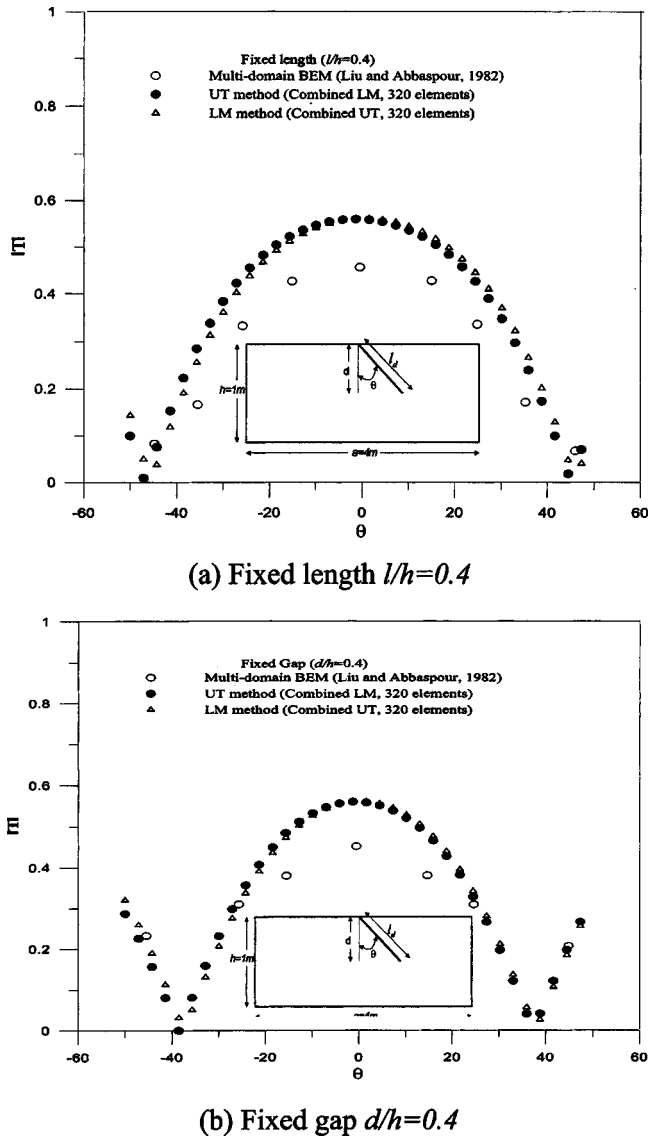

Fig. 10. Transmission coefficients versus different inclination angles of thin breakwater: (a) fixed length $l_d/h=0.4$ and (b) fixed gap $d/h=0.4$ (case 2, $kh=2.075$)

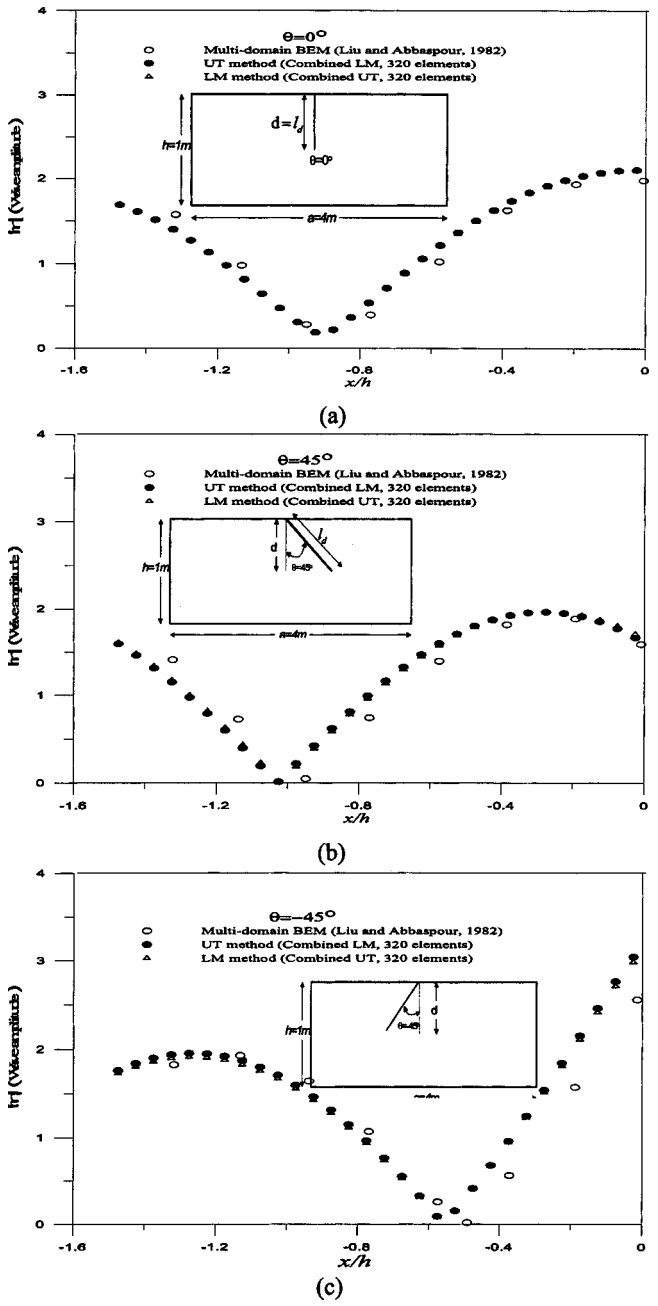

Fig. 11. Wave amplitude on front side of thin breakwater: (a). $\theta=0°$, (b) $\theta=45°$, and (c) $\theta=-45°$ (case 2, $kh=2.075$, $d/h=0.4$)

revealed. The energy-loss index, $E_L=1-(R^2+T^2)$, for the energy dissipation versus kh with respect to the different porous coefficients is plotted in Figs. 15 ($G=0.5$) and 16 ($G=1.0$), respectively. Fig. 17 displays the energy-loss index E_L versus kh for $G=0.5$ and 1, to see the dissipation efficiency due to porous parameters. The results by using LM-DBEM, which are not good enough for the higher wave number by using constant elements to capture hypersingularity, can be attributed to the same number of boundary elements for all cases of the different wave numbers. Indeed, we need to refine the mesh to improve the better result or to employ a higher-order element as shown in Fig. 12.

Case 4: Submerged Breakwater with Absorbing Boundary Condition

Numerical results were displayed to examine the validity of a thin submerged breakwater with absorbing boundary condition by varying different absorbing coefficients on the front and back sides of the breakwater. To ensure the current numerical computation's accuracy, the numerical results of the eigenfunction expansion method are also shown for comparison. According to numerical experiments, the length of each pseudoboundary is also adopted by double the water depth. In this case, the submergence ratio (d/h) is also 0.75 the same as Case 3. By using the dual formulations (*UT* or *LM* methods), the reflection and transmission coefficients are plotted against kh in Figs. 18 and 19 for $(G_1,G_2)=(0.5,0.0)$ and (1.0, 0.0) in Eqs. (9) and (10). The results are compared well with those of the eigenfunction expansion method. To see the dissipation efficiency due to a different absorbing instrument in the front side of the breakwater, transmission and reflection coefficients for different absorbing coefficients, $(G_1,G_2)=(0.0,0.0)$, (0.5, 0.0), (1.0, 0.0), versus kh by using the *UT* method are shown in Fig. 20. Fig. 21 indicates the reflection and transmission coefficients using the DBEM and

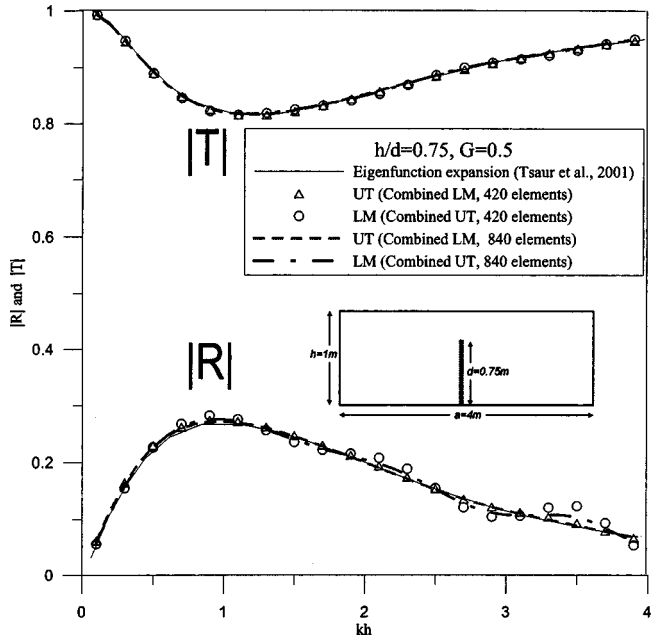

Fig. 12. Transmission and reflection coefficients obtained by using different methods (case 3, $h/d=0.75$, $G=0.5$)

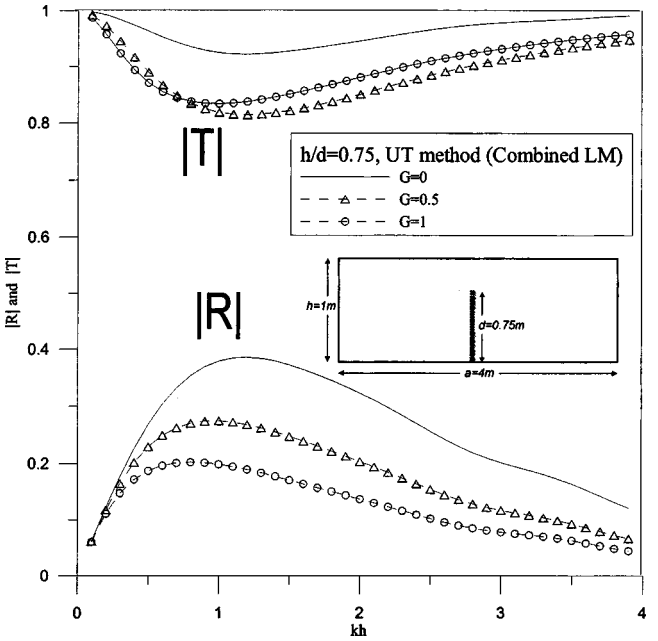

Fig. 14. Transmission and reflection coefficients for different porous coefficients obtained by using *UT* method (combined *LM*) (case 3, $h/d=0.75$, $G=0,0.5,1.0$)

eigenfunction expansion method against *kh* with $(G_1,G_2)=(1.0,1.0)$, of which the two absorbing instruments for two absorbing coefficients, G_1 and G_2, are set in the front side and back sides of the breakwater. The results agree well with those of the eigenfunction expansion method. To display the dissipation efficiency due to different absorbing instruments in the back side of the breakwater, transmission and reflection coefficients for different absorbing coefficients $(G_1,G_2)=(1.0,0.0),(1.0,\ 0.5),(1.0,\ 1.0)$ versus *kh* are shown in Fig. 22 by using the *UT* method. The physical phenomenon of energy-loss dependency on different absorbing materials on the front or back sides of the breakwater is clearly revealed. The value of transmission coefficient is larger when the absorbing coefficient G_2 is larger. The energy-loss index E_L of energy dissipation versus *kh* for the absorbing coefficient $(G_1,G_2)=(1.0,1.0)$ is plotted in Fig. 23. Fig. 24 shows the energy-loss index E_L versus *kh* for $(G_1,G_2)=(0.0,0.0)$, (0.5, 0.0), (1.0, 0.0), to see the dissipation efficiency due to different absorbing instruments in the front of the breakwater.

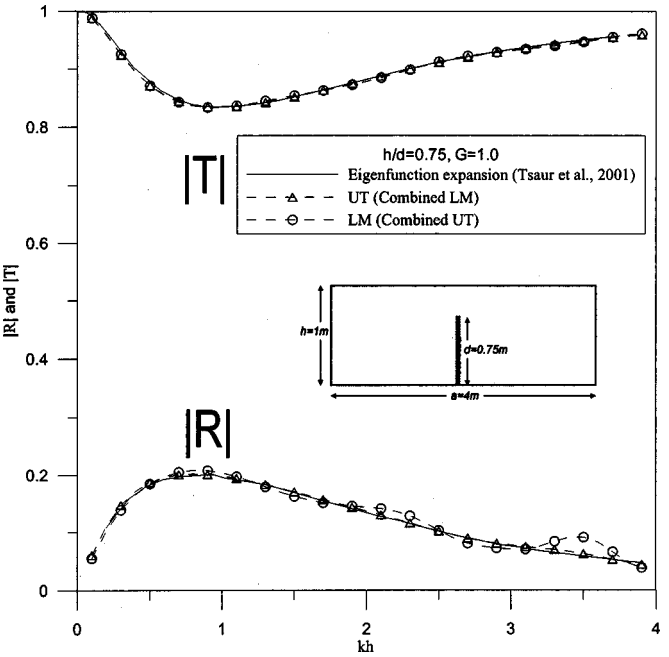

Fig. 13. Transmission and reflection coefficients obtained by using different methods (case 3, $h/d=0.75$, $G=1$)

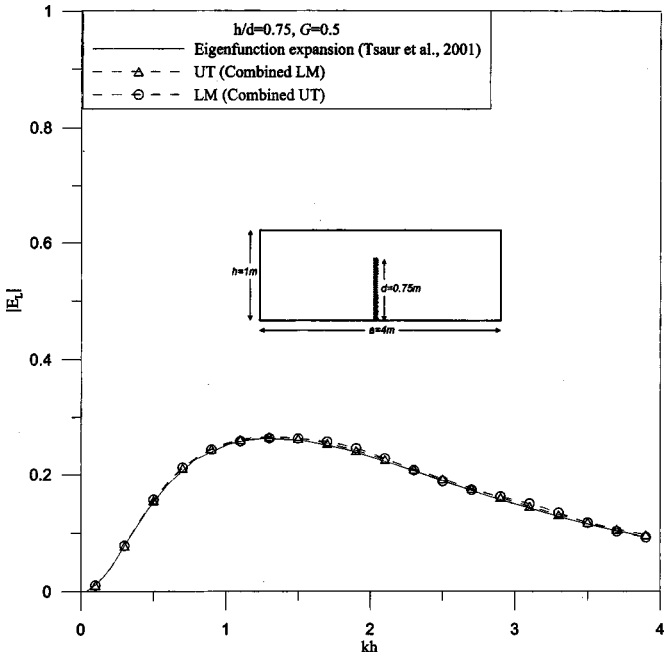

Fig. 15. Energy-loss coefficients obtained by using different methods (case 3, $h/d=0.75$, $G=0.5$)

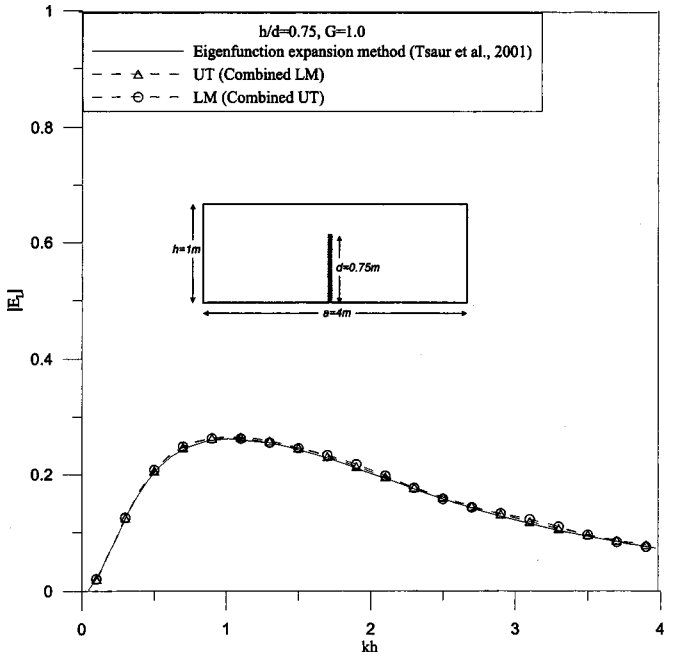

Fig. 16. Energy-loss coefficients obtained by using different methods (case 3, $h/d=0.75$, $G=1.0$)

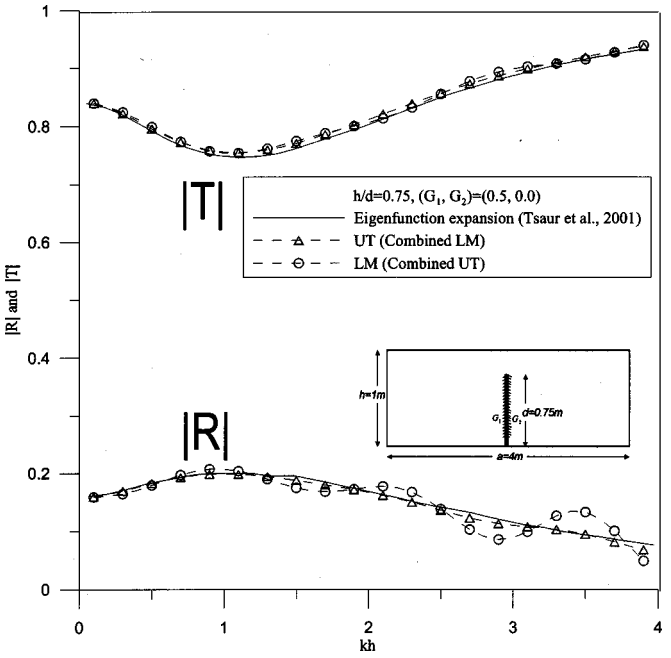

Fig. 18. Transmission and reflection coefficients obtained by using different methods [case 4, $h/d=0.75$, $(G_1,G_2)=(0.5,0.0)$]

Conclusions

The dual integral formulation for solving the propagation of incident wave passing a vertical and inclined thin barrier with rigid boundary condition which is descending from the water surface to a depth, and a thin vertical submerged breakwater with absorbing or porous boundary conditions which is extending from the seabed to a height has been derived in this paper. The drawback of the multidomain approach is obvious in that the artificial boundary is arbitrary, and thus not qualified as an automatic scheme. For the computational efficiency, a larger system of equations is required since the degrees of freedoms on the interface are put into the system, and it takes more CPU time and memory space than the DBEM method to solve the linear algebraic equation. For the accuracy, the DBEM result is better than multidomain BEM by comparing that of the eigenfunction expansion method. A DBEM program has been developed to solve for this scattering

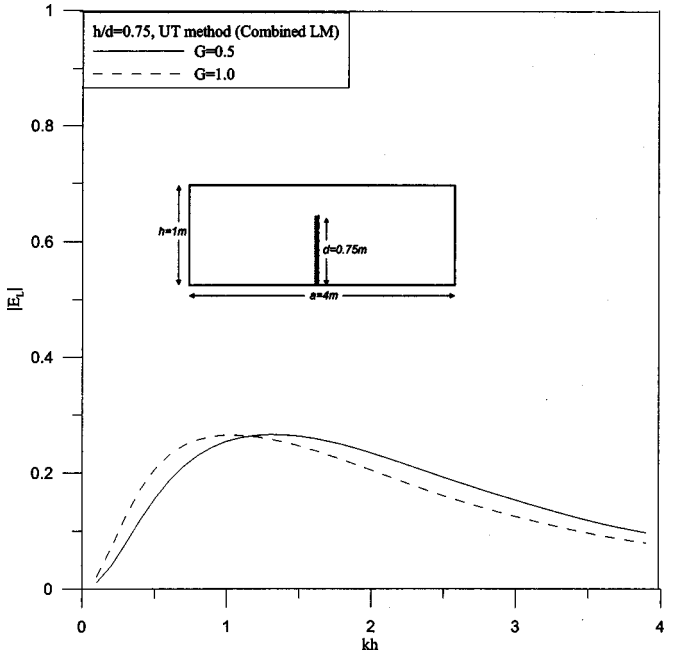

Fig. 17. Energy-loss coefficients obtained for different porous coefficient by using *UT* method (combined with *LM* method) (case 3, $h/d=0.75$, $G=0.5,1$)

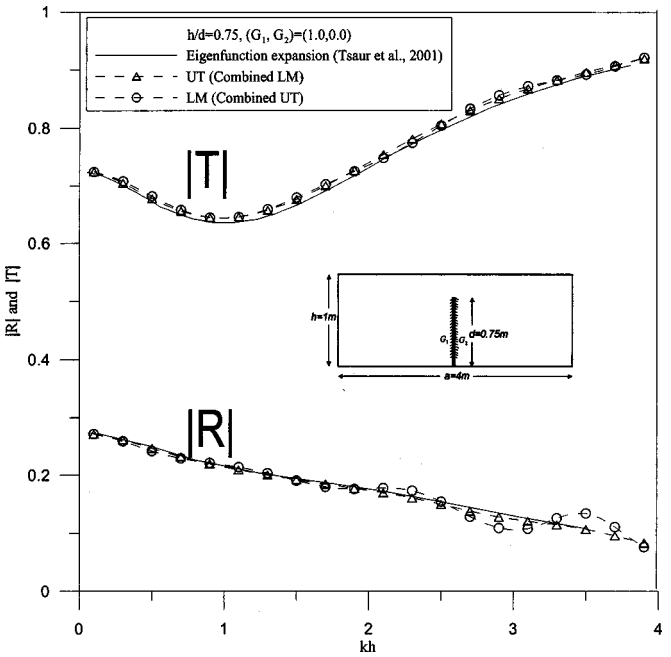

Fig. 19. Transmission and reflection coefficients obtained by using different methods [case 4, $h/d=0.75$, $(G_1,G_2)=(1.0,0.0)$]

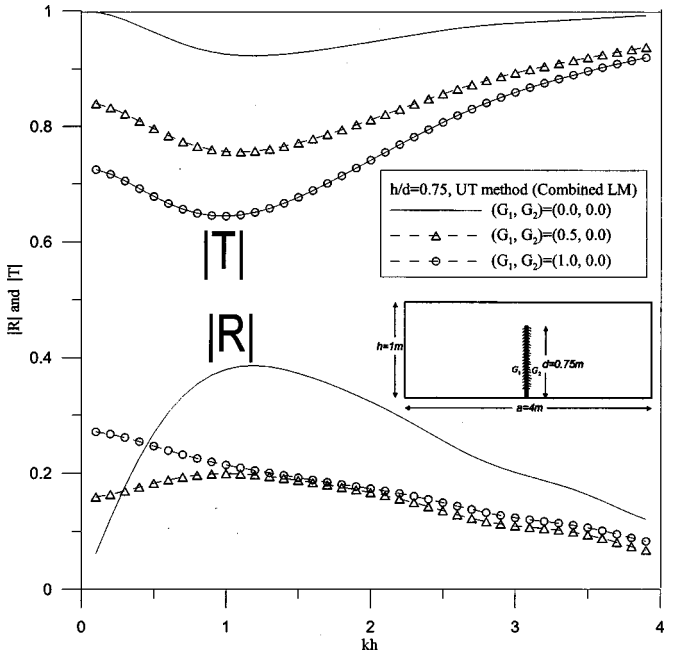

Fig. 20. Transmission and reflection coefficients for different absorbing coefficients obtained by using *UT* method (combined with *LM* method) [case 4, $h/d=0.75$, $(G_1,G_2)=(0.0,0.0)$, $(0.5,0.0)$, $(1.0,0.0)$]

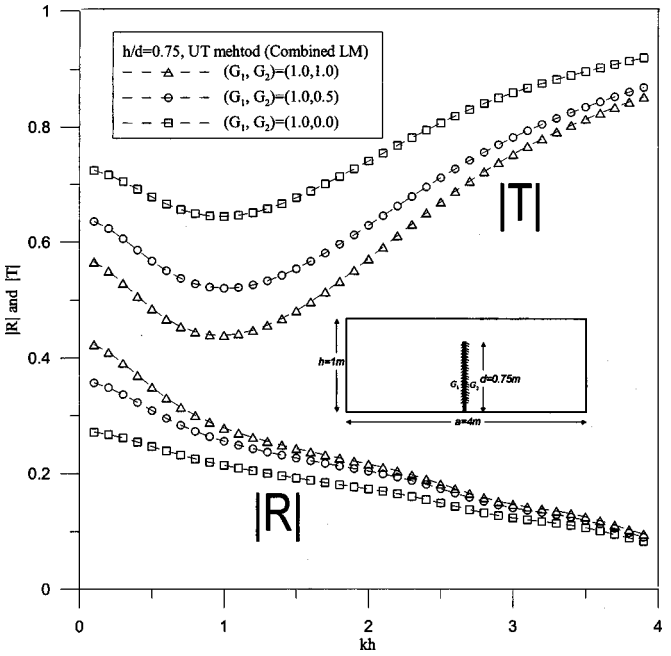

Fig. 22. Transmission and reflection coefficients for different absorbing coefficients obtained by using *UT* method (combined with *LM* method) [case 4, $h/d=0.75$, $(G_1,G_2)=(1.0,0.0)$, $(1.0,0.5)$, $(1.0,1.0)$]

problem. Four illustrative examples of thin (zero thickness) barriers with rigid, porous, and absorbing boundary conditions, have been successfully solved using the proposed DBEM, and the results were compared well with those obtained using analytical solutions, numerical solutions of the multidomain BEM, and experiments.

Acknowledgments

Financial support from the National Science Council, Grant No. NSC-91-2211-E-019-010 to National Taiwan Ocean Univ., and the scholarship of Sinotech Foundation for Research and Development to the first writer are gratefully acknowledged.

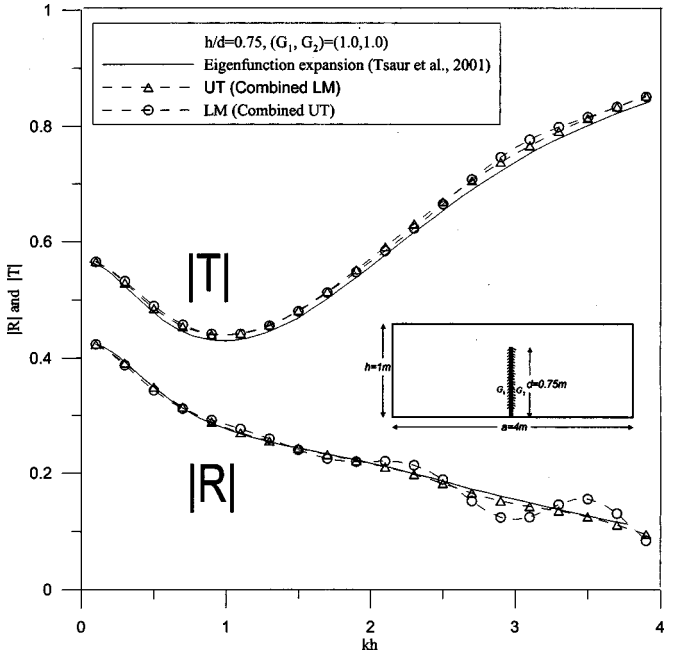

Fig. 21. Transmission and reflection coefficients obtained by using different methods [case 4, $h/d=0.75$, $(G_1,G_2)=(1.0,1.0)$]

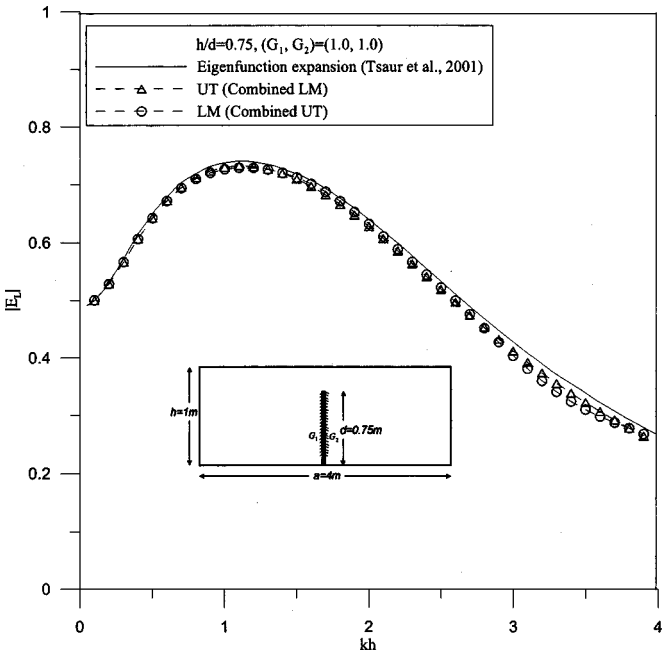

Fig. 23. Energy-loss coefficients obtained by using different methods [case 4, $h/d=0.75$, $(G_1,G_2)=(1.0,1.0)$]

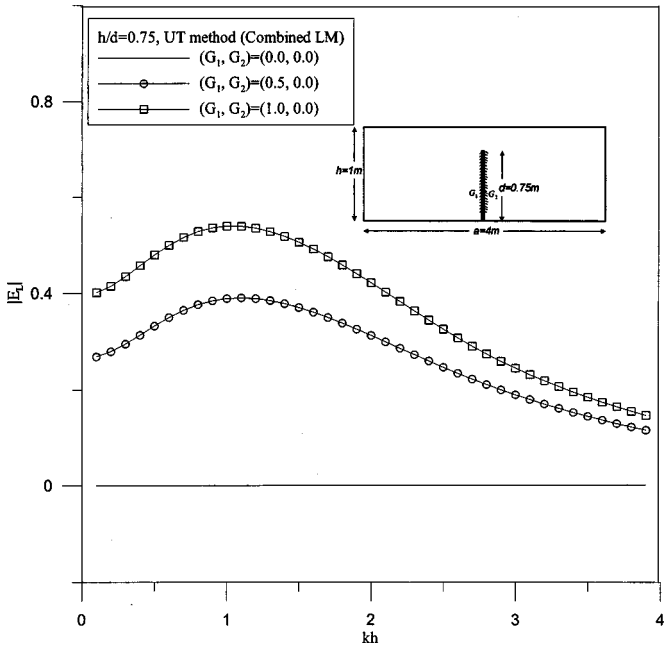

Fig. 24. Energy-loss coefficients obtained by using *UT* method for different absorbing coefficients [case 4, $h/d=0.75$, $(G_1,G_2)=(0.0,0.0),(0.5,0.0),(1.0,0.0)$]

Notation

The following symbols are used in this paper:

A = amplitude of incident wave;
D = domain of interest;
$dB(\tilde{s}_j)$ = jth integration element;
G = complex porous-wall-effect parameter;
G_1 = absorbing parameters of front side of breakwater;
G_2 = absorbing parameters of back side of breakwater;
g = acceleration of gravity;
h = water depth;
k = wave number;
l_d = length of elements on barrier;
n = boundary normal vector;
n_d = total numbers of elements on barrier;
$n_{\tilde{s}}$ = normal vector at boundary point $\tilde{s}$;
R = reflection coefficient;
$\tilde{s}$ = source point;
s_i = coordinate of boundary node on barrier;
T = transmission coefficient;
U = fundamental solution;
$\tilde{x}$ = field point;
$\tilde{x}_i$ = ith collocation point;
δ = dirac-delta function;
σ = wave frequency; and
Φ = velocity potential.

References

Aliabadi, M. H. (1997). "Boundary element formulations in fracture mechanics." *Appl. Mech. Rev.*, 50, 83–96.

Aliabadi, M. H., and Saleh, A. L. (2002). "Fracture mechanics analysis of cracking in plain and reinforced concrete using the boundary element method." *Eng. Fract. Mech.*, 69(2), 267–280.

Blandford, G. E., Ingraffea, A. R., and Liggett, J. A. (1981). "Two-dimensional stress intensity factor computations Using the Boundary Element Method." *Int. J. Numer. Methods Eng.*, 17, 387–404.

Chen, K. H., Chen, J. T., Chou, C. R., and Yueh, C. Y. (2002). "Dual boundary element analysis of oblique incident wave passing a thin submerged breakwater." *Eng. Anal. Bound. Elem.*, 26(10), 917–928.

Chen, J. T., and Hong, H.-K. (1993). "On the dual integral representation of boundary value problem in Laplace equation." *Bound. Elem. Abstracts*, 3, 114–116.

Chen, J. T., and Chen, K. H. (1998). "Dual integral formulation for determining the acoustic modes of a two-dimensional cavity with a degenerate boundary." *Eng. Anal. Bound. Elem.*, 21, 105–116.

Chen, J. T., and Hong, H.-K. (1999). "Review of dual boundary element methods with emphasis on hypersingular integrals and divergent series." *Appl. Mech. Rev.*, 52(1), 17–33.

Chen, J. T., Lin, S. R., Chen, K. H., Chen, I. L., and Chyuan, S. W. (2003). "Eigenanalysis for membranes with stringers using conventional BEM in conjunction with SVD technique." *Comput. Methods Appl. Mech. Eng.*, 192, 1299–1322.

Dean, R. G., and Dalrymple, R. A. (1984). *Water wave mechanics for enginers and scientists*, Prentice-Hall, Englewood Cliffs, N.J.

Hong, H.-K., and Chen, J. T. (1988). "Derivations of integral equations of elasticity." *J. Eng. Mech.*, 114(6), 1028–1044.

Hsu, H. H., and Wu, Y. C. (1999). "Scattering of water wave by a submerged horizontal plate and a submerged permeable breakwater." *Ocean Eng.*, 26, 325–341.

Jones, D. B., Lee, J.-J., and Raichlen, F. (1979). "A transportable breakwater for nearshore application." *Proc., Specialty Conf. Civil Engineering in Ocean IV*, Vol. 1, 433–456.

Lafe, O. E., Montes, J. S., Cheng, A. H. D., Liggett, J. A., and Liu, L.-F. (1980). "Singularities in Darcy flow through porous media." *J. Hydraul. Div., Am. Soc. Civ. Eng.*, 106(6), 977–997.

Lee, M. M., and Chwang, A. T. (2000). "Scattering and radiation of water by permeable barriers." *Phys. Fluids*, 12, 54–65.

Linton, C. M., and McIver, P. (2000). "Green's functions for water waves in porous structures." *Appl. Ocean. Res.*, 22, 1–12.

Liu, P. L. F., and Abbaspour, M. (1982). "Wave scattering by a rigid thin barrier." *Proc. Am. Soc. Civ. Eng.*, 108, 479–491.

Losada, I. J., Losada, M. A., and Roldan, J. (1992). "Propagation of oblique incident waves past rigid vertical thin barriers." *Appl. Ocean. Res.*, 14, 191–199.

Losada, I. J., Patterson, M. D., and Losada, M. A. (1997). "Harmonic generation past a submerged porous step." *Coastal Eng.*, 31, 281–304.

McIver, P. (1999). "Water-wave diffraction by thin porous breakwater." *J. Waterw., Port. Coastal, Ocean Eng.*, 125(2), 66–70.

Raichlen, F., and Lee, J.-J. (1978). "An inclined plat wave generator." *Proc., 16th Coastal Engineering Conf.*, 388–399.

Sommerfeld, A. (1964). "Lectures on theoretical physics." *Partial differential equations in physics*, Vol. VI, Chap. 28, Academic, New York.

Tsaur, D. H., Yueh, C. Y., Chang, K. H., and Yang, Y. C. (2000). "A study on wave scattering by submerged plate-type breakwater with absorbing boundary." *Proc., 12th Hydraulic Engineering Conf.*, Taiwan, R.O.C., 168–174 (in Chinese).

Ursell, F. (1974). "The effect of a fixed vertical barrieron surface waves in deep water." *Proc. Cambridge Philos. Soc.*, 43(3), 374–382.

Wiegel, R. L. (1960). "Transmission of wave past a rigid vertical thin barrier." *J. Waterw. Harbors Div., Am. Soc. Civ. Eng.*, 86, 1–12.

Wu, Y. C., Hsu, R. C., and Chen, J. C. (1999). "The interaction of oblique wave with submerged porous breakwaters." *Proc., 21th Ocean Engineering Conf.*, Taiwan, R.O.C., 259–266 (in Chinese).

Yip, T. L., and Chwang, T. (1998). "Water wave control by submerged pitching porous plate." *J. Eng. Mech.*, 124(4), 428–434.

Yu, X. (1995). "Diffraction of water waves by porous breakwaters." *J. Waterw., Port. Coastal, Ocean Eng.*, 121(6), 275–282.